MECHANICAL PROPERTIES OF LIME-TREATED SOIL AND ITS APPLICATION TO EARTHEN WALLS

Jina LEE[1], Junichi KOSEKI[2], Takeshi SATO[3],
Tsutomu NAMIKAWA[4] and Hiroyuki ARAKI[5]

ABSTRACT: In order to investigate the resistance and seismic behavior of a natural building material obtained by compacting a mix of soil, lime and water, shear and tensile properties are evaluated by conducting a series of compaction, unconfined compression, unconfined tension and drained triaxial tests. Moreover, a finite element analysis is conducted, based on an elasto-plastic model describing both the shear and tensile properties of the material, in order to determine the maximum stresses and identify the possible failure pattern.

Key Words: lime-mixed soil wall, tensile strength, earth construction, water to lime ratio

INTRODUCTION

Earthen constructions have been built for more than thousands years and today are still homes, to between a third and a half of the world's population. To ensure protection of their inhabitants, especially in highly seismic zones, there is a need of reinforcing these structures. As a matter of fact, even though those earth buildings are very durable, some standing for more than hundred years, recent earthquakes (Iran 2003, Peru 2007, Pakistan 2008) have shown the need of ensuring a better resistance of the structures to earthquakes as numerous deaths occurred as a result of their collapse.

Moreover, there is today a renewed interest in studying the earth constructions in a context of growing environmental awareness promoting a reduction of our impact on our planet and health. Rammed earth is considered to be a good sustainable alternative to current construction practices as it is sustainable, cost-effective, regulates the internal humidity and enables to conserve and pass on a cultural heritage. There is a strong tradition of earthen walls in Japan, and some earth constructions were preserved as a precious heritage like the walls surrounding Horyu-ji temple which is listed as a UNESCO World Heritage site (**Figure 1**).

In this study, a natural construction material inspired by a traditional Japanese technique called "Shikkui" is being studied for the construction of the rammed earth walls of a low energy house. It is obtained by mixing the silty sand of the waste of the future construction site, quicklime and water; compacting and finally air-curing it. The addition of lime because of the high seismicity and risks of other natural disasters such as heavy rains, typhoons of the area classifies the technique as stabilized rammed earth.

---

[1] Formerly master student, Department of Civil Engineering, University of Tokyo
[2] Professor, Institute of Industrial Science, University of Tokyo
[3] Technical Director, Integrated Geotechnology Institute Ltd.
[4] Associate Professor, Department of Civil Engineering, Kobe City College of Technology
[5] Ph.D. student, Department of Civil Engineering, University of Tokyo

Figure 1. Rammed earth wall surrounding Horyu-ji temple, Hyogo Prefecture, Japan

In order to investigate the resistance and seismic behavior of the lime-mixed soil, shear and tensile properties are evaluated. After determining the optimum proportions of the mixture by performing compaction tests, case L and case M (in which there is twice less lime than case L) were determined, in which the water was added at their optimum content w_{opt}, and the sand/gravel ratio was kept constant. A series of unconfined compression tests, drained triaxial tests and unconfined tension tests was performed using a triaxial apparatus in order to evaluate the strength and deformation characteristics of the material. Finally a finite element analysis using a simple elasto-plastic model is used to better understand the failure characteristics of the lime-mixed soil wall.
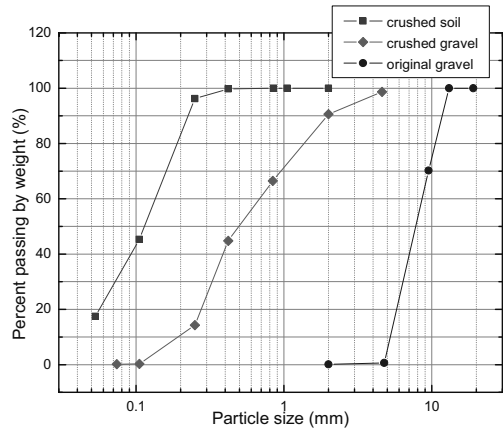
TEST CONDITIONS AND PROCEDURES

The tested material is obtained by mixing at two different ratios (cases L and M, **Table 1**):

- The soil retrieved from a future construction site in Chiba Prefecture, Japan, composed of a silty sand (Gs=2.67 and D_{max} =0.42 mm)
    - Particles of gravel
    - Commercial lumps of quicklime (CaO)
    - Water

Preliminary unconfined compression tests, where four different soil/water/lime ratios (cases A through D) were defined by an experienced building professional showed that one mixture, case A, was the most adequate because it exhibited higher compressive peak strength (3 MPa) after a 56 days curing period at a dry density of 1.70 g/cm^3.

Figure 2. Particle size distribution of the materials

The composition of case A is also shown in **Table 1**. After performing unconfined compression tests on the samples (100 mm in height, 50 mm in diameter), it was decided to crush the original soil into the clean silty sand, along with a "crushed" version of the gravel, which is classified as a poorly graded sand, due to the possible particle size/scale effect on the estimation of the strength of the material. As a matter of fact, the large particles of gravel could entice localized failure given that the specimen is with dimensions of 10 cm in height and 5 cm in diameter. Its particle size distribution is also visible on **Figure 2**.

The moulding water content w_m, defined by Miura et al. (2001), as the ratio of the amount of water introduced to the dry weight of solid (soil and lime) is equal to 25.2 %. It is higher than the initial water content w_i which is the water content measured immediately after compaction, as water is absorbed by the hydration reaction and evaporated because of its exothermicity. The lime content l, defined as the lime to soil ratio by dry weight is equal to 22.7 %.

Based on these results, Modified Proctor compaction tests (E=2700 kJ/m^3) were performed in order to find an optimum lime/water ratio, for a mixture keeping the sand/gravel ratio with a similar lime content in case L (l=22.7 %) and another case M using a half of this lime content (l=11.4 %) in a perspective of cost and energy reduction. The compaction curve (**Figure 3**) shows that with the addition of lime, the water content increases as more water is needed to achieve the chemical reactions which will strengthen the mix. On the other hand, the maximum dry density decreases thus resulting in poorer compaction conditions. For the new mixtures in cases L and M, the water was added at their optimum content w_{opt}

Figure 3. Compaction curves of lime-soil mixtures with l=11.4 % and 22.7 % at Ec=2700 kJ/m^3

of 20.0 % and 20.5 % respectively, corresponding to moulding water contents w_m of 30.2 % and 24.1 %.

Table 1. Mixing proportions of materials of cases A, L, M

Case	A		L		M	
	Volume ratio	Weight in percentage(%)	Volume ratio	Weight in percentage(%)	Volume ratio	Weight in percentage(%)
Soil*	4	55.9	4	53.8	4	61.8
Gravel*	0.5	9.1	0.5	8.8	0.5	10.1
Lime	1	14.8	1	14.2	0.5	8.2
Water	1.67	20.1	2	23.2	1.5	20.0

* original soil and gravel were mixed in the preliminary tests and crushed soil and gravel for cases L and M

UNCONFINED COMPRESSION TESTS

The crushed original soil and crushed gravel were first mixed with water, and then the lime was added and thoroughly mixed. As the reaction is exothermic, the compaction began after 15 minutes to allow the mix to cool down. The blend was put in a sealed container during the preparation of the samples in order to avoid variation of the moisture content.

Each specimen was compacted in a plastic mould with a dimension of 50 mm in inner diameter and 100 mm in height, into ten layers. Based on the weight and dropping height of the rammer, the required number of blows was assigned in order to apply the same energy of compaction as in the modified Proctor test.

The samples were then cured inside their moulds without sealing under atmospheric pressure and room temperature to simulate the actual conditions, for 6 different curing periods: 7, 14, 28, 56, 84 and 140 days. For each mixture and curing time, 3 samples were made.

After the curing period, the samples were demoulded, and unconfined compression tests were performed. In order to reduce the effects of bedding error at the interfaces between the specimen and

the top cap and pedestal, a capping was made by applying gypsum. A constant strain rate of compression was set to 1 %/min and the axial displacement was measured by two LVDTs (Linear Variable Displacement Transducers) set at diametrally opposed positions.

UNCONFINED TENSION TESTS

The preparation of the mixture is identical to the unconfined compression tests, while the specimen shape and dimensions are modified; they are cylindrical with a diameter of 50 mm and a height of 140 mm and the diameter at the middle height was trimmed down to 45 mm as shown in **Figure 4**. The dimensions of the specimen was modified based on the results from finite element analyses (Koseki et al., 2005) in order to avoid failure at the fixed portions in which the tensile stress may be concentrated to a large extent.
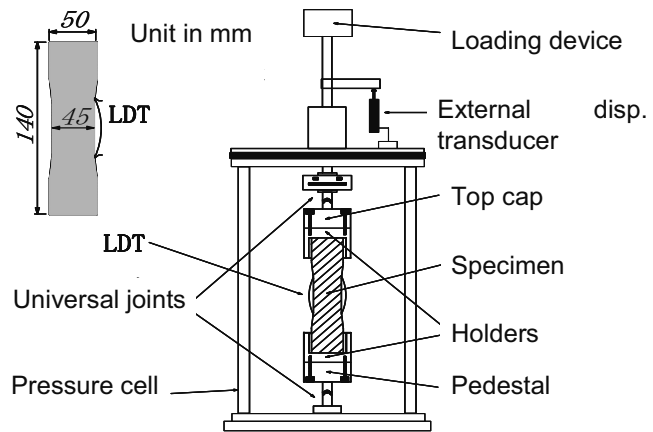
The trimming was operated by a private company which requested us to compact the specimen in a special acrylic mould with a larger diameter of 55 mm in order to facilitate the trimming process, after several specimens with an initial diameter of 50 mm were broken during the process. It is noted that the specimen may have been altered during the preparation as the trimming process entailed a prolonged sealing in plastic wrap and disturbance resulting from:

- friction between the acrylic mould and the lime-soil mixture during demoulding process

Figure 4. Apparatus for unconfined tension test and specimen dimensions

- the trimming process itself which used a metallic roller while pouring water and fixing both ends with glue to the machine. Out of the 14 specimens sent to the company, three were broken and two were ill-trimmed.
- the transportation of the specimens to and from the company:

The apparatus developed by Koseki et al (2008) shown in **Figure 4** was used, without using the pressure cell. It can transfer tensile force to the specimen by using gypsum as a filling material in the gap between the specimen and its holders. The holders were attached to the top cap and the pedestal, while universal joints were inserted on both ends to reduce the bending moment applied unnecessarily to the specimen.

A pair of local deformation transducers (LDTs) was attached on the trimmed section and two diametrally opposed external transducers (LVDTs) were placed at the top of the apparatus. A tensile load was applied to the specimen at a nominal axial strain rate of -0.01 %/min.

During the setting of the specimen in the apparatus, special care was taken in order to keep the specimen centered and horizontal. In spite of that, it was difficult to keep a null eccentricity which most probably altered the tensile failure of the specimens.

TEST RESULTS –UNCONFINED COMPRESSION TESTS–

The relationships between the deviator stress q which in this case is equal to the axial compressive stress under unconfined stress state, and the externally measured axial strain for cases L and M are shown in **Figure 5** It can be seen that:

- in both cases, the peak strength of the lime-mixed soil is increasing with the curing period, even after 28 days, suggesting that, like cement-mixed sandy soils (Kongsukprasert et al., 2007) and contrary to concretes, the strength value at 28 days does not reflect the material's actual strength over a long period of time. After a curing period of two months, the peak strength q_u was 35% and 53% higher than that of 28 days for cases L and M, respectively. After three months, the peak strength seems to stabilize in both cases, indicating that in case of lime-soil mixes, the peak strength at 56 days is to be taken into account for design.

- the failure strain mobilized at the peak stress state is between 1 to 3%, and seems to decrease with the increase in curing period.

- the initial secant stiffness increases over the curing period, which is more visible with case M. This change in the stiffness could be explained by the decrease of water content over time as will be shown in **Figure 6** (b).
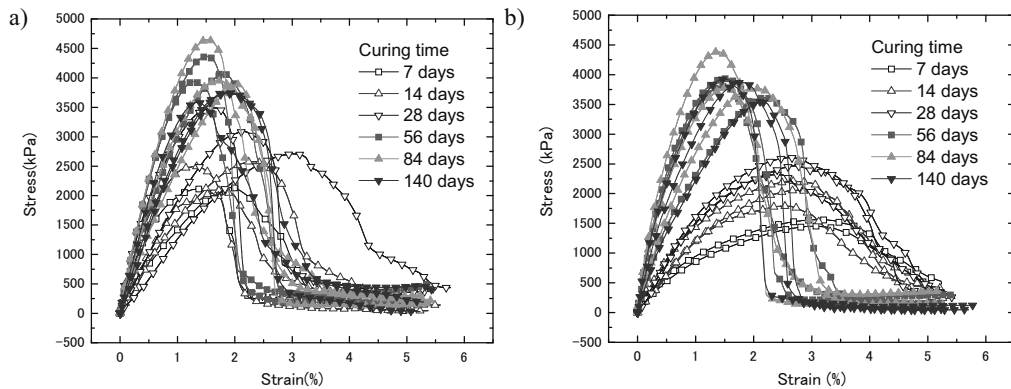
Figure 5. Stress-strain relationships of (a) case L and (b) case M for curing periods from 7 to 140 days
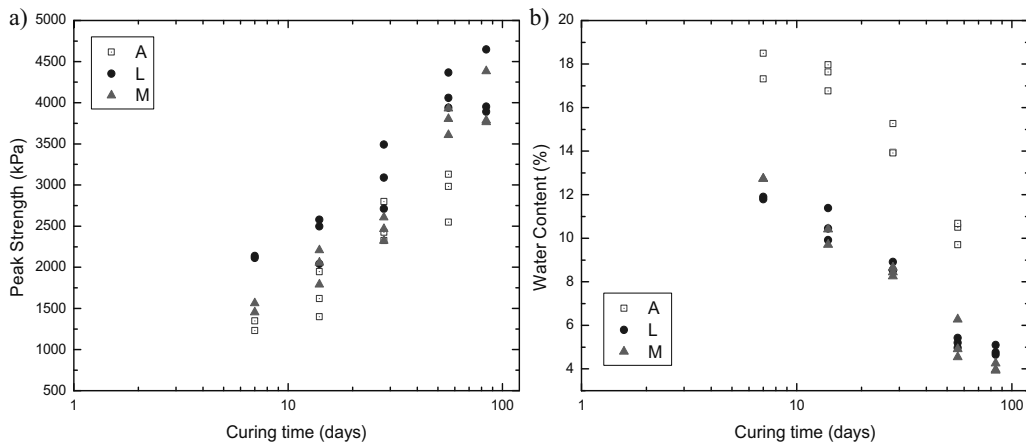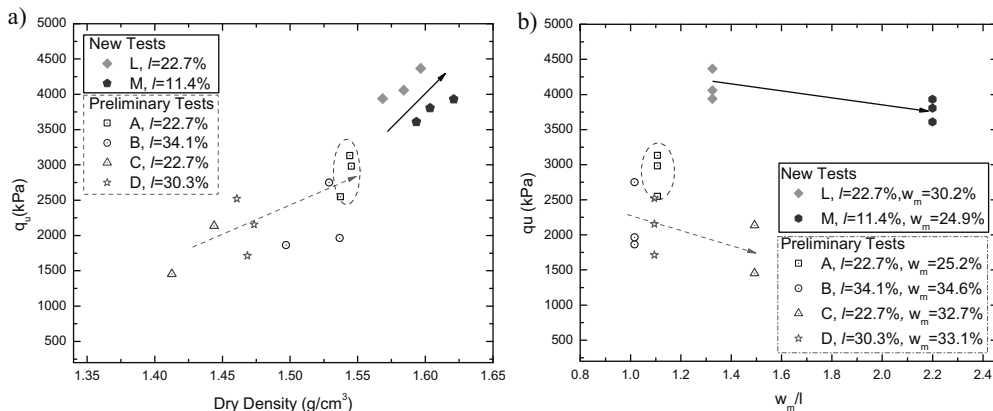

Figure 6. (a) Peak strength and (b) water content measured after testing in function of the curing time

Figure 6, which illustrates the peak strength and the water content that was measured after the test plotted against the logarithm of the curing time, clearly reveals the strengthening behavior of the lime-mixed soil with time. Until t=28 days, cases A and M exhibit a similar peak strength and case L has a higher one, but for t=56 days, it can be seen that cases L and M reach similar higher values than case A. Their water content values being lower, and their dry density being higher than that of case A, we could conclude that both new mixtures are more adequate than case A concerning their peak strength.

Case M has half the amount of lime than case L, while it exhibits a q_u value that is similar to the one of case L. The mixture M would be preferred in constructing the soil wall, for it will enable savings in terms of costs and energy.

Figure 7 shows the influence of the dry density and of w_m/l defined as the water content to lime content ratio on the peak strength of the lime-mixed soils, including the other preliminary test results at a curing time of 56 days. It can be seen for both the preliminary and the new tests that the peak strength increases with the dry density and decreases when w_m/l increases (except for case A which will be explained later). The two series of tests cannot be compared directly to each other as the materials used, the compaction energy and the curing conditions are not identical.

Figure 7. Peak strength in the cases L and M and in the preliminary test cases A, B, C, D at t=56 days in function of (a) dry density and (b) w_m/l (the water content to lime content ratio)

It should be noted in **Figure 7** (b) that the mix in case A exhibits a higher strength than cases B, C and D. Case A and C having the same lime content (22.7%), this could be explained by the lower moulding water content of case A, thus better compaction conditions, than the other ones

The mix in case D which has higher contents of water and of lime than A, exhibits a lower strength than A, indicating that for a given w_m/l, an excessive amount of water or lime is detrimental to the specimen's strength.

Under given conditions with respect to the material used, compaction energy and curing conditions, these parameters, dry density and w_m/l give us a useful tool that can help determine an adequate ratio of the mixture with sufficient peak strength.

TEST RESULTS –UNCONFINED TENSION TESTS–

The relationships between the deviator stress q which in this case is equal to the axial tensile stress under unconfined stress state, and the axial strain measured with the external transducer (LVDT) and the local deformation transducers for cases L and M are shown in **Figure 8** and **Figure 9**. The strain

and stress are positive in tension in the following graphs.

a)

b)
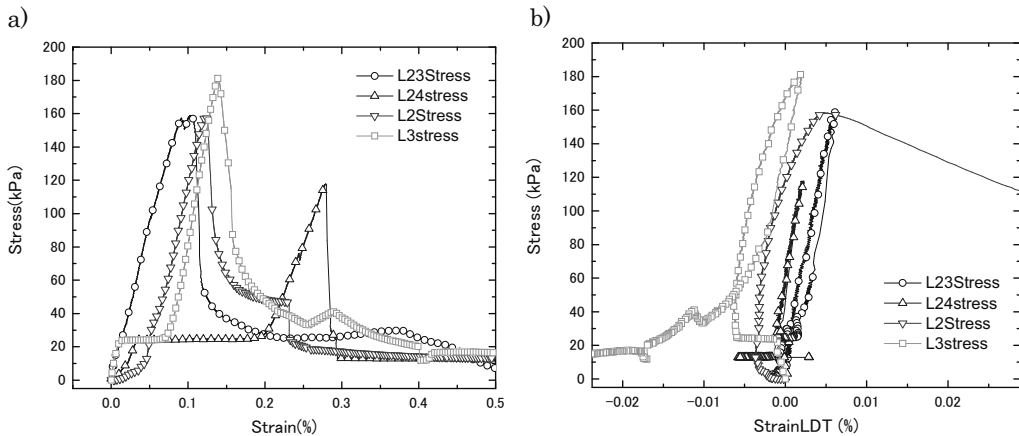
Figure 8. Stress-strain relationship by (a) LVDTs and (b) LDTs for case L

It can be seen that:
- the peak strengths are low and scattered
- the stress-strain curves in the unconfined tension tests based on local and external deformation measurements are very different from each other. The axial strains measured with the LVDT attached at the top cap are overestimated, as they include the effects of bedding errors at the interfaces between the specimen and the top cap and the pedestal and the effects of other system compliances such as the deformation of the loading shaft and the universal joints. The horizontal levels that can be seen in most of the cases after the initial loading part are due to these errors linked to the equipment.
- the residual stress state mobilized at a strain level of about 0.5 % by external measurement is low, around 20 kPa for both cases.
- the failure strains mobilized at the peak stress state range from 0.1 to 0.2% by external measurement for both cases after correction for the horizontal levels induced by the apparatus errors. The local strains at failure are smaller than 0.01% which is ten times less than the external ones: the importance of using local deformation measurements in accurately evaluating the failure strain level is highlighted.

a)

b)
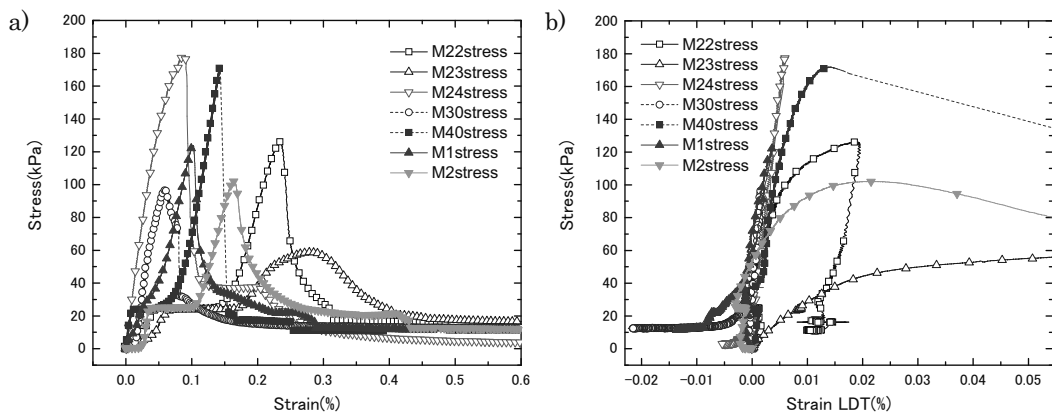
Figure 9. Stress-strain relationship by LVDT (a) and LDTs (b) for case M

Comparison with the results of the unconfined compression and tension tests
The results of unconfined compression and tension tests are compared. It is to be noted that the curing conditions being different, the specimens do not have the exact same properties.

The peak strengths are plotted in **Figure 10** and compared to those of the unconfined compression tests. The average peak tensile strengths are 154 kPa for case L and 122 kPa for case M. The average peak strengths in the unconfined compression tests were 3098 kPa and 2465 kPa respectively. The tensile strength values thus represent only 5% in both cases, of the compressive strength ones. These values are lower than those found by Koseki et al. (2008) on cement-treated sands (mixing proportions for cement/water/sand being similar to those of lime/water/soil) after a curing period of seven days, which ranged from 20 to 30% of the unconfined compression strength for a shorter curing period, as can be seen in **Figure 10** (b). For a curing period three times higher than that of the cement-treated sands, the tensile strength for the lime-treated soil is three to six times lower.
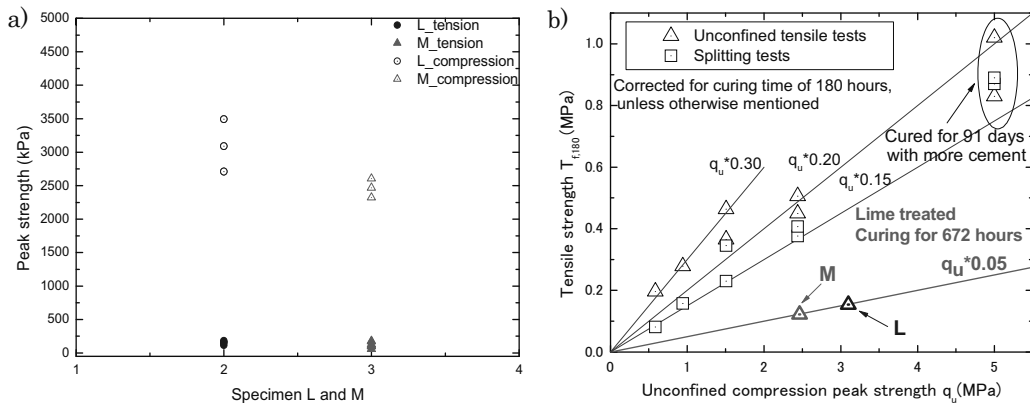

Figure 10. (a) Relationships between unconfined tensile strengths and compressive strength; (b) comparison with cement-treated sands (modified after Koseki et al., 2008)

If the tensile strength is indeed so low, it would not be possible to use these materials without reinforcements. However, the disturbance due to the errors due to the characteristics of the apparatus and the specimen preparation process could highly affect its tensile behavior. More repeatable tests should be conducted where the specimen disturbance and scatter are reduced to its minimum.

The tensile crack is formed normal to the direction of the tensile stress as can be seen in **Figure 11**.

- Most of the overall failure of the specimens occurred at the trimmed part of the specimen, but not necessarily within the length of the LDTs.

- For some specimens, the specimen failed at the level of the border of the holders, which may suggest that the failure was enhanced by a bending moment resulting from an off-center loading due to the misalignment of the specimen. The actual strength of the material could thus have been affected.
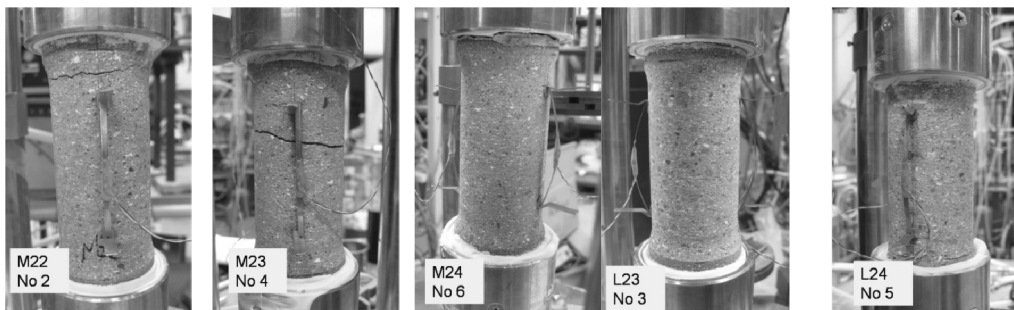
Figure 11. Specimens M22, M23, M24 and L23, L24 after the unconfined tension tests

The location of the tensile crack of the specimens may be linked to the interfaces between the compacted layers. **Figure 12** (a) shows the X-ray images of one specimen before the trimming process: although each layer was "disturbed" manually after its compaction in order to ensure the cohesion between particles with those of the next layer and homogeneity of the specimen, it is clearly visible that the interfaces and the outer areas of the specimens are less dense (shown by dark gradation in **Figure 12**). The interfaces can be a likely failure area during tension tests. **Figure 12** (b) shows that one specimen which was broken during the trimming process at one of those interfaces.
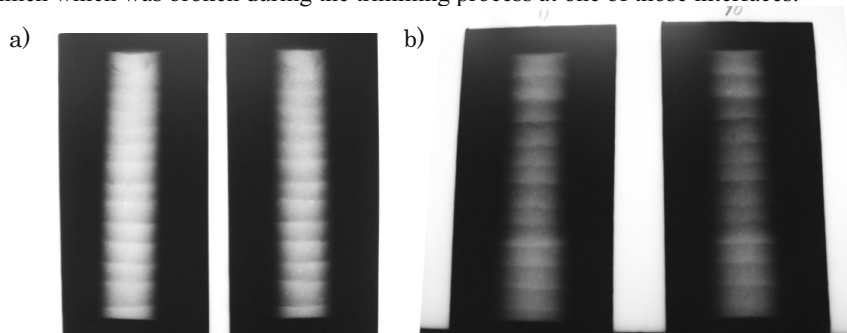
Figure 12. X-ray images of (a) one specimen before the trimming process and (b) another specimen after it broke during the trimming process (by courtesy of OYO corporation)

For the numerical analysis: in a conservative approach, the tensile strengths and Young's modulus of 100 kPa, 100 MPa for case M and 150 kPa, 200 MPa for case L, respectively, were assigned.

FINITE ELEMENT ANALYSIS

The seismic behavior of a lime-mixed soil wall section is investigated using a 2D finite element analysis and incorporating experimentally obtained properties of cases L and M (Elastic modulus, tensile strength, angle of internal friction, cohesion, etc.) with previously presented tests and drained triaxial tests. An elasto-plastic model developed by Namikawa and Mihira (2007) appropriately describing the non-linear shear and tensile behaviors of cement-treated soils was used.

The new model is built based on various laboratory test results (Koseki et al., 2008), i.e., triaxial compression, triaxial tension, plane strain compression, direct tension, splitting and bending tests, and within the framework of a relatively simple elasto-plastic theory.

Two failure criteria are employed to express tensile and shear failure characteristics observed in the experimental results of the cement-treated sands. It can describe strain-hardening and strain-softening responses in both failure modes. In the strain softening rules, the smeared crack concept is used and a characteristic length is considered to avoid the issue of mesh-size dependency.

This model was used to simulate the behavior of cement-treated sand in the laboratory tests, and it was shown to be suitable to describe the tensile and shear failure behaviors of cement-treated sands. The formulation of the model is not explained in this paper and can be found in Namikawa et al (2007).

The finite element mesh that was employed is shown in **Figure13**. The dimensions are those of the cross section of the soil wall present in Horyu-ji temple (**Figure 1**). The height of the wall is 2400 mm, the top length 1100 mm and the bottom length 1400 mm. It is composed of 8400 elements of around 20*20 mm² and 8591 nodes, each row being divided into 70 elements. The definition of coordinates is also shown in **Figure 13**.
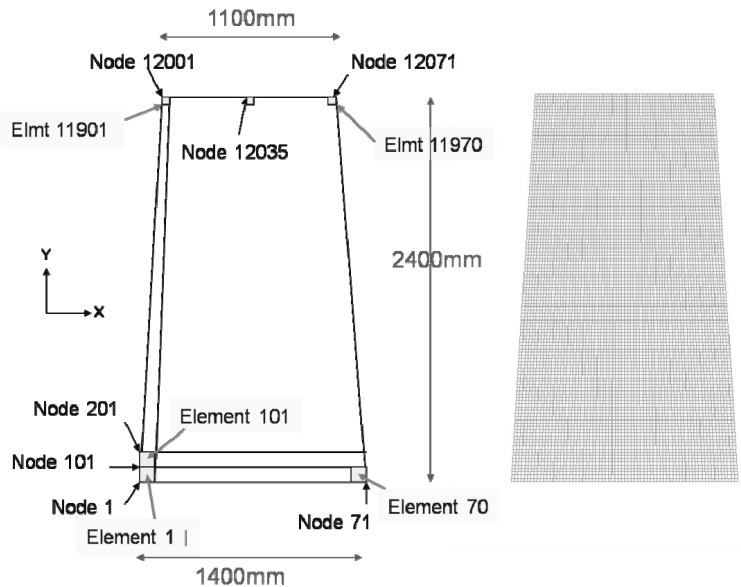
Figure 13. Mesh used in numerical analysis of the seismic behavior of lime-mixed soil wall

The boundary conditions and loads are as follows:

- At the base, the first row is fixed in XY direction
- A damper base was added, so that the seismic waves are not trapped in the soil wall and can be dissipated into the ground.
- Roof load was modeled by a beam element at the top of the wall, with an intensity of 3.31 kPa using a small elastic modulus (E=10 MPa).
- Self-weight of the wall was considered

The N-S component of the recorded earthquake motion at Kobe JMA (Japan Meteorological Agency) station during the 1995 Hyogoken-Nanbu earthquake was used as the base input motion for the analysis. The input motion (**Figure 14**) was applied laterally in the x direction and the duration of the excitation was 20 seconds. When necessary, the input motion was modified by rescaling the maximum acceleration to obtain information about the influence of the maximum acceleration.
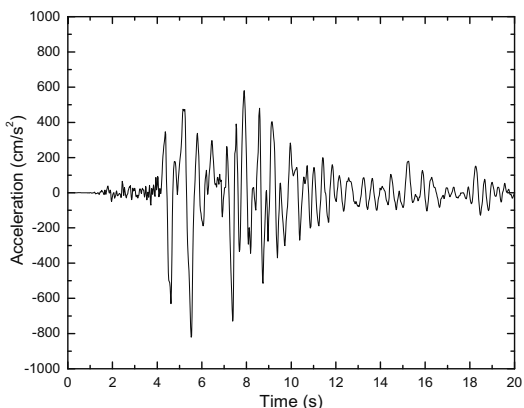
Figure 14. Input motion for horizontal excitation at the base of the wall, α_{max} =821cm/s²

Material Parameters of the elasto-plastic model

The parameters to enter in the program (Namikawa and Mihira, 2007) are listed in **Table 2**. The first part of the table consists of the input parameters obtained by the previously detailed tests. The parameters in the second part of the table are made on some assumptions that are explained below.

Table 2. Material parameters in the elasto-plastic model

		L	M
Experimentally deduced parameters			
Elastic modulus	E (MPa)	200	100
Tensile strength	T_f (kPa)	150	100
Angle of internal friction	$\phi(°)$	35.3	40.7
Cohesion	c (kPa)	983	758
Density	$\rho(g/cm^3)$	1.70	1.75
Assumed parameters			
Poisson's ratio	ν	0.33	0.33
Hardening parameter	a	1.05	1.05
Hardening parameter	e_y	0.0002	0.0002
Fracture energy	G_f (N/m)	37.5	37.5
Softening parameter	e_r	0.40	0.40
Dilatancy coefficient	D_c	-0.4	-0.4
Localization size	t_{s0} (mm)	0.6	0.6
Characteristic length	l_c (mm)	20.0	20.0
Damping coefficients	α	2.10	1.47
	β	0.000133	0.000190

The fracture energy $G_f (N/m)$ is an important parameter dominating the tensile softening behavior. It enables to accurately evaluate the softening relation and the peak load. It was obtained for cement-treated sand by Namikawa and Koseki (2006) from the results of three-point bending tests.

The parameters e_r and D_c are related to the shear fracture energy and to the dilation during the shear strain softening process, respectively. They were evaluated by plane strain compression tests (Namikawa and Mihira, 2007).

$t_{s0} (mm)$ is related to the size of strain localization zone and is assumed to be 0.6 mm which is the value obtained in the plane strain compression tests by Namikawa and Koseki (2006).

l_c is determined from the mesh size.

The viscous Rayleigh damping was employed as the material damping. C=α M+ β K where M, C and K are the mass, damping and stiffness matrices and α, β the damping parameters. As the damping matrix C functions depend on the frequency, these parameters were obtained by an eigen value analysis while assuming the modal damping factor of the Rayleigh damper $h_r = 1/2 (\alpha/w_r + \beta \cdot w_r)$ =0.02 at the first and second dominant frequencies of the wall (case L: f_1=11 Hz and f_2=37 Hz; case M: f_1=8 Hz and f_2=26 Hz).

Results of finite element analysis

By inputting the properties presented above, the walls failed: numerical analysis could not be successfully completed as the number of iterations increased significantly as too many elements failed for the duration of the strong motion. It was thus decided to vary the value of the tensile strength T_f and the maximum acceleration α_{max} of the input motion in order to evaluate for which value failure would take place. When the analysis could not be completed, a new analysis was run with a lower

maximum acceleration.

The maximum values of the minor principal stress in tension, $\sigma_{3,max}$, mobilized at the bottom corner of the wall (Element 1, **Figure 13**) are plotted versus the maximum acceleration α_{max} in **Figure 15**. It can be seen that:

- Failure occurred when $\sigma_{3,max}$ exceeded the tensile strength in case L.

- In case L with T_f =150 kPa, partial failure could be observed when α_{max} was higher then 500 cm/s², and it was followed by the overall failure that took place when α_{max} was higher than 650 cm/s². It is to be noted that $\sigma_{3,max}$ was equal to 156 kPa when α_{max} =650 cm/s².

- In M case, shear failure occurred before $\sigma_{3,max}$ reached the tensile strength.

- In case M with T_f =100 kPa, partial failure began to occur when α_{max} was higher then 350 cm/s², and overall failure occurred when α_{max} was higher than 400 cm/s². It is to be noted that $\sigma_{3,max}$ was equal to 90 kPa when α_{max} =400 cm/s².
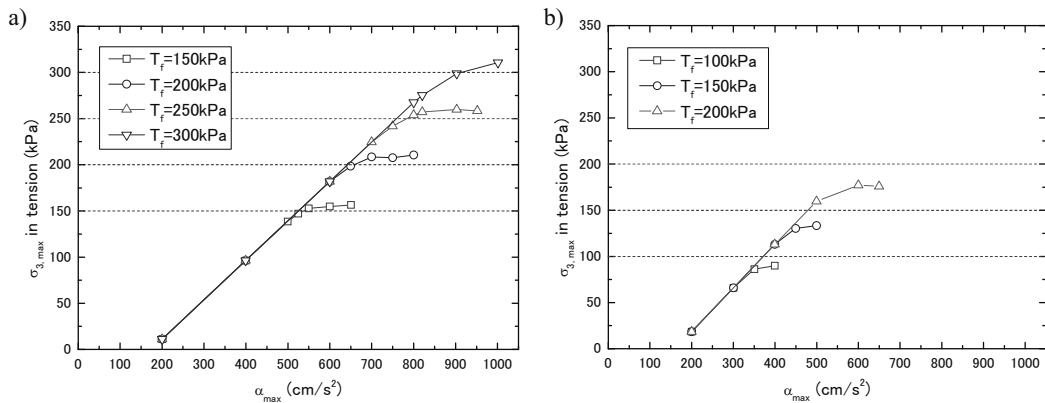
Figure 15. Maximum values of minor principal stress in function of α_{max} for (a) case L and (b) case M
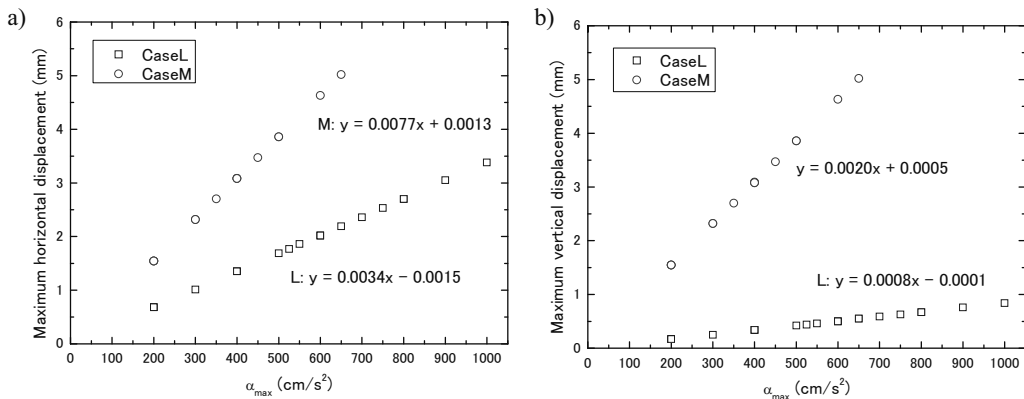
Figure 16. Maximum (a) horizontal and (b) vertical displacements in function of α_{max} for cases L and M

The maximum horizontal and vertical displacements at the top corner of the wall (Node 12001,

Figure 13) were plotted also in function of α_{max} in **Figure 16**. The displacements are very small compared to the dimensions of the wall. Moreover, there is a linear relationship with the maximum acceleration, even when partial failure occurs. These observations suggest that the wall response is more like a rigid body.

Figure 17 plots the time history of the minor principal stress, in a certain case denoted as case 1 (case L with T_f =150 kPa and α_{max} =650 cm/s²) at the element 1 which is at the left bottom corner of the wall. It can be seen that the minor principal stress exceeded the tensile strength slightly at two points.
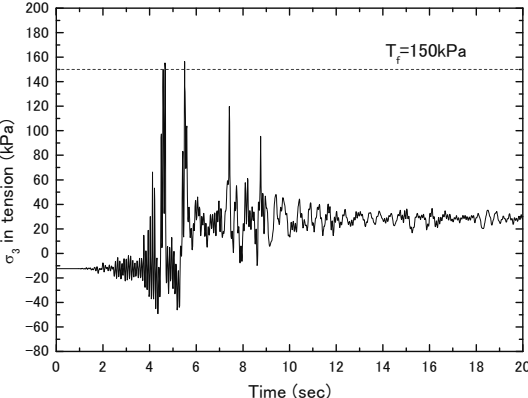

Figure 17. Time history of minor principal stress at elements 1 in case 1 (case L with T_f =150 kPa and
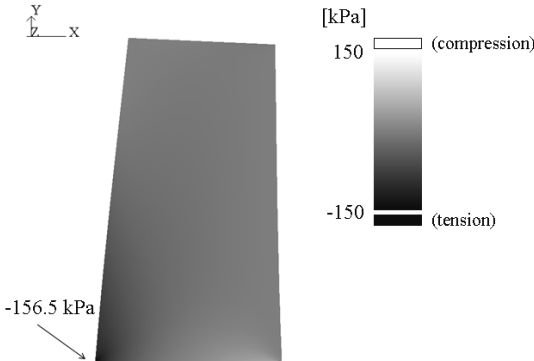
α_{max} =650 cm/s²)

Figure 18. Distribution of the minor principal stress at t= 5.5 s in case 1

The distribution of the minor principal stress is shown in **Figure 18** for the above case 1 at t=5.5 second, when the input acceleration exhibits nearly the maximum value (=650 cm/s²). At this time of the shaking, $\sigma_{3,max}$ values reach the tensile strength T_f of the wall, and partial failure takes place at the bottom corners of the walls where the tensile stresses are localized as can be seen in the figure. It is to be noted that in all the figures the displacements of the shown wall were enlarged by 50 times.

The distribution of the vertical displacement is shown in **Figure 19** (a) for the same case 1. The rocking motion of the wall can be clearly seen.

The distribution of the horizontal displacement is shown in **Figure 19** (b). The displacements relative to the base are very limited. The maximum horizontal displacement at the top of the wall was 2.2 mm, which was about 0.09 % of the wall height (=2400 mm)
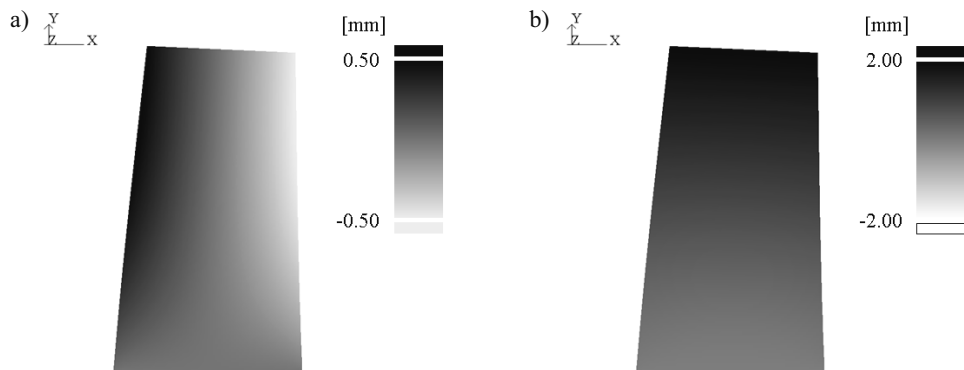
Figure 19. Distribution of (a) vertical displacement and (b) horizontal displacement at t= 5.5 s in case 1

CONCLUSIONS

The unconfined compression tests revealed the strengthening properties of a lime-soil mixture even after 28 days of curing time. It was shown that by compacting the mixtures at two different lime contents 11.4% and 22.7% at their optimum water content values, the shear strength properties are similar to each other, leading us to prefer the former mixture as a more economical solution. This study revealed the importance of a good compaction of the mixture and of a proper water to lime ratio.

The unconfined tension tests revealed low tensile peak strengths: representing only 5% of the compressive strength after the same curing time for both cases. It is questioned whether the specimens were affected by the sample preparation as the compaction of the specimen in different layers may have led to weak interfaces, the trimming process may have further weakened the specimen, and the curing conditions were not the same as in the unconfined compression tests.

The finite element analysis using an elasto-plastic model for the soil wall showed that considering the N-S component of the recorded earthquake motion at Kobe JMA (Japan Meteorological Agency) station during the 1995 Hyogoken-Nanbu earthquake as the base input motion, the walls would be subjected to an overall failure due to their low tensile strengths (case L: T_f =150 kPa; case M: T_f =100 kPa). Reinforcements should thus be considered under these proportions conditions.

The effects of varying the values of the maximum acceleration α_{max} and the tensile strength T_f of the material were studied through a series of finite element analyses. In the above cases L and M, partial failure is induced at α_{max} =500 and 350 cm/s^2, respectively, which develops into overall failure at α_{max} =650 and 400 cm/s^2.

ACKNOWLEDGEMENTS

REFERENCES

Kongsukprasert, L., Tatsuoka, F. and Takahashi, H. (2007): Effects of curing period and stress conditions on the strength and deformation characteristics of cement-mixed soil, Soils and

Foundations, 47(3), 577-596.

Koseki, J., Sato, T., Mihira, S., Takeya, N. and Yoshizawa, M. (2005): Comparison of tensile strength of cement treated sand by various test methods, Proc. of International Conference on Deep Mixing, CD-ROM.

Koseki, J., Tsutsumi, Y., Namikawa, T., Mihira, S., Salas-Monge, R., Sano, Y. and Nakajima, S. (2008): Shear and tensile properties of cement-treated sands and their application to liquefaction mitigation, Keynote Lecture, Proc. of 4th International Symposium on Deformation Characteristics of Geomaterials (IS-Atlanta 2008), 1, 27-50.

Miura, N., Horpibulsuk. and Nagaraj, T.S. (2001): Engineering behavior of cement stabilized clay at high water content, Soils and Foundations, 41(5), 33-45.

Namikawa T. and Koseki, J. (2006): Experimental determination of softening relations for cement-treated sand, Soils and Foundations, 46(4), 491-504.

Namikawa T. and Mihira, S. (2007): Elasto-plastic model for cement-treated sand, International Journal for Numerical and Analytical Methods in Geomechanics, 31, 71-107.

Namikawa T. and Koseki, J. (2007): Evaluation of tensile strength of cement-treated sand based on several types of laboratory tests, Soils and Foundations, 47(4), 657-674.